Interlayer coupling within individual submicron magnetic elements

David J. Smith,[a),b),f)] R. E. Dunin-Borkowski,[b),c)] M. R. McCartney,[b)] B. Kardynal,[d),e)] and M. R. Scheinfein[a)]
Arizona State University, Tempe, Arizona 85287

(Received 22 November 1999; accepted for publication 10 February 2000)

The interlayer coupling and magnetization reversal of patterned, submicron Co/Au/Ni nanostructures, shaped as diamonds, ellipses, and rectangles, have been investigated using off-axis electron holography and micromagnetic simulations. Antiferromagnetic coupling between the ferromagnetic layers, attributed to the strong Co demagnetization field, was visualized directly. Simulated hysteresis loops overall showed reasonable agreement with the experimental results. Local structural imperfections may be responsible for small discrepancies between the observed magnetization states of the patterned elements and the simulations. © *2000 American Institute of Physics.* [S0021-8979(00)04010-X]

I. INTRODUCTION

Quantitative characterization of magnetization reversal mechanisms in submicron-sized magnetic elements is essential for the future development of high-density, magnetic information storage systems. The behavior of thin continuous films, which can be studied by bulk characterization methods, is rarely a reliable guide for predicting the properties of small magnetic elements of well-defined size and shape.[1] The formation of edge domains in patterned submicron elements strongly influences their switching fields,[2] while the shape anisotropy of magnetic tunnel junctions (MTJs) dominates their hysteretic response.[3] The magnetic interactions between two thin, closely separated, ferromagnetic (FM) layers within individual lithographically defined structures, such as MTJs or spin valves, can also influence their switching mode and coercive field. Changes in the separation of the FM materials and their parallel or antiparallel magnetic alignment can cause substantial changes in electrical resistance when the magnitude and direction of an externally applied magnetic field is varied. This effect is commonly termed giant magnetoresistance (GMR).[4]

We have previously shown that off-axis electron holography is a powerful experimental tool for the characterization of magnetic interactions associated with patterned Co nanostructures.[5,6] Here, we apply this technique to investigate magnetization reversal in magnetically asymmetric, Co/Au/Ni patterned trilayer structures with approximate lateral dimensions of between 100 and 300 nm. We also compare our experimental measurements with simulated domain distributions determined from solutions to the Landau–Lifshitz–Gilbert (LLG) equations.[7]

II. EXPERIMENTAL DETAILS

The elements examined here consisted of Co/Au/Ni trilayers patterned into diamonds, ellipses and rectangular bars. They were prepared directly onto self-supporting 55-nm-thick silicon nitride membranes using electron-beam lithography and lift-off processes. Individual trilayer elements were well separated laterally in order to reduce inter-element magnetic interactions.[6] Electron holograms were recorded at 200 kV using a Philips CM200 transmission electron microscope equipped with a field-emission electron gun. In addition to an electrostatic biprism for generating electron holograms, the instrument was equipped with an additional (Lorentz) minilens which allowed holograms to be recorded at magnifications of up to $\sim 70kx$ and resolutions of ~ 2 nm with the objective lens switched off and the sample located in nearly field-free conditions.[8] The objective lens could also be excited slightly so that magnetization processes and hysteresis loops could be followed *in situ* by tilting the specimen in a known, previously calibrated, magnetic field.[5] Figure 1(a) shows a low magnification bright-field image of one array of patterned shapes, while the schematic diagram in Fig. 1(b) shows the nominal cross-sectional structure of each element. The representative electron hologram in Fig. 1(c) illustrates the typical lateral dimensions of the nanostructures, which are thin rectangular bars in this example. The corresponding smaller and larger diamonds and ellipses had similar heights as the bars, and widths of 120 or 160 nm. In all of the experimental results reported below, the contribution of the mean inner potential to the holographic phase was subtracted from the holograms in order to obtain the magnetic contribution of primary interest.[9]

Micromagnetic simulations incorporated room temperature simulation parameters for Co (and Ni), including the exchange stiffness, $A = 1.55$ (and 0.80 for Ni) μerg/cm and the saturation magnetization, $M_s = 1414$ (and 440 for Ni) emu/cm^3. The magnetocrystalline anisotropy constant, K, in our polycrystalline layers (below 10 nm grain size) was set

[a)]Department of Physics and Astronomy, Arizona State University, Tempe, AZ 85287-1504.
[b)]Center for Solid State Science, Arizona State University, Tempe, AZ 85287-1704.
[c)]Present Address: Department of Materials, Parks Road, Oxford OX1 3PH, UK.
[d)]Center for Solid State Electronics Research, Arizona State University, Tempe, AZ 85287.
[e)]Present Address: Clarendon Laboratory, Parks Road, Oxford OX1 3PU, UK.
[f)]Electronic mail: david.smith@asu.edu

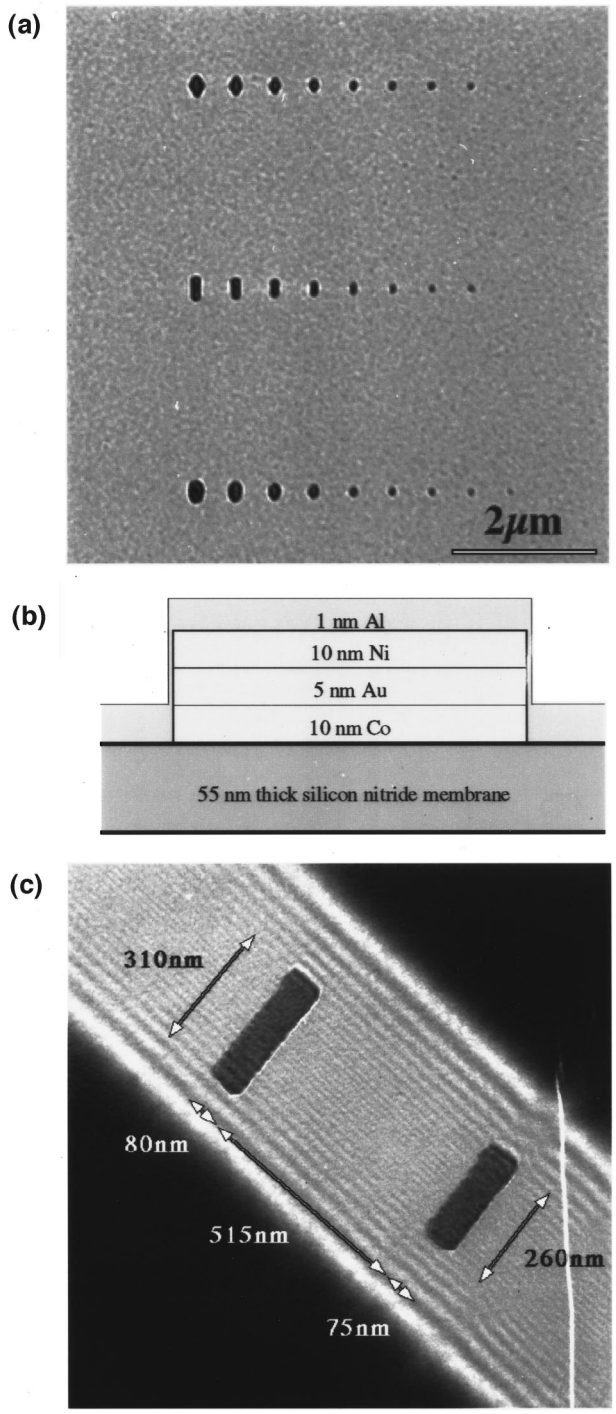

FIG. 1. Experimental configuration. (a) Low magnification image showing array of small patterned elements in the form of diamonds, rectangles, and ellipses; (b) schematic cross section showing nominal vertical dimensions of Co/Au/Ni trilayer structure. The thin Al overlayer was intended to provide protection against oxidation and to prevent charging of the sample during observation in the electron microscope. (c) Electron hologram of two rectangular bars showing typical lateral dimensions.

to zero. A value for K of 0 is consistent with the observation that the coercivity in our elements (ascribed to shape anisotropy) is much larger than that typical of bulk films of the same thickness, implying that magnetocrystalline anisotropy plays a minor role in the energetics of switching. A gyromagnetic frequency, $\gamma = 17.6\,\mathrm{MHz/Oe}$, and a damping constant, $\alpha = 1$, were used in the LLG calculations, and the effects of temperature fluctuations were not included. In-plane, discrete moments (representing a continuous magnetization distribution) were 5.0 nm on each side, and a single layer of moments was used for each magnetically active layer. The demagnetization field was computed to all orders, coupling the moments in all cells with each other. Magnetization reversal processes were followed by assigning an initial domain structure and then integrating the LLG equations in a fixed external field until equilibrium was reached. The exit criteria corresponded to the largest change in the residual direction cosine of all discretized moments in the grid changing by less than 2×10^{-5}.

III. RESULTS AND DISCUSSION

Representative results for a selection of the elements are tabulated in three sets of four columns in Fig. 2. The left column of each set shows a selection of the experimental results in the form of the magnetic contributions to the experimental holographic phases during a complete hysteresis cycle. In these observations, the in-plane field (shown at left) was varied along the vertical direction of the figure between $\pm$ 1930 Oe (corresponding to $\pm$ 30° sample tilt) in an out-of-plane field of 3600 Oe. The different directions of the measured in-plane magnetization are represented by a continuous color wheel, in which the directions in the plane of the film are blue (up), red (right), yellow (down), and green (left). The intensity of the colors reflects the magnitude of the in-plane magnetization. The holographic phase contours, which have a spacing of 0.064π radians, follow lines of constant magnetic induction (**B**-field strength): Their separation is proportional to the in-plane component of the magnetic induction integrated in the incident beam direction. Although the data are noisy due to the underlying silicon nitride membrane, the contours can still be followed both inside the elements and in the surrounding magnetic leakage fields. The emergence of phase contours from the sides of the diamonds and ellipses over substantial portions of the hysteresis cycle indicates that interactions between neighboring elements would occur if they were placed in close proximity.

The experimental results in Fig. 2 show that the switching fields needed for complete magnetization reversal of the diamond- and elliptical-shaped elements are smaller than for the rectangular bar. A solenoidal vortex state is visible for the elliptical shape during both forward and reverse cycles (at -168 and $+336$ Oe). Simulations were unable to replicate this vortex structure despite extensive trial-and-error attempts, suggesting that structural imperfections may have been a contributing factor.[10] Vortex states were also seen in the smaller diamond-shaped elements but they were never observed in the rectangular bars, presumably because of the narrow dimensions and the dominant influence of shape anisotropy on the magnetic response.[3] Significantly, the bars are also too thin and narrow to form end-domains, which govern the reversal of larger rectangular elements.[11–13] Instead, the phase contours typically curve at their ends by a maximum angle of $\sim 45°$ just before magnetization reversal

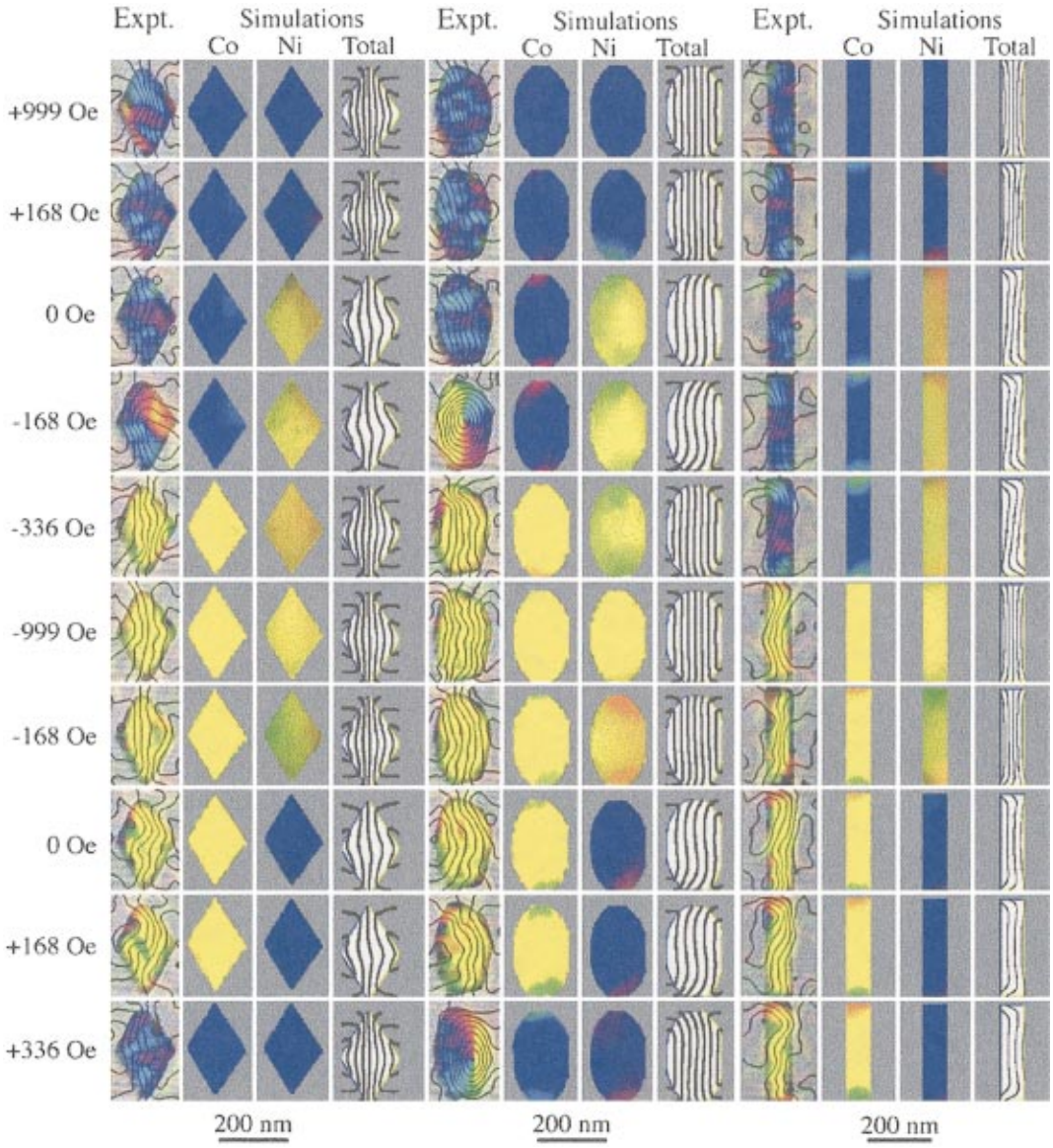

FIG. 2. (Color) Comparison of experimental and simulated magnetization states during complete hysteresis cycles for patterned Co/Au/Ni spin-valve elements in the form of diamonds, ellipses, and rectangular bars. Applied in-plane fields (in vertical direction on page) are shown at left. Experimental phase contours are separated by 0.064π radians. Columns labeled ''Co'' and ''Ni'' are simulations for the individual FM layers, and those labeled ''total'' are simulations for the composite Co/Au/Ni structure.

(see, for example, the +336 Oe image of the rectangular bar at the bottom of Fig. 2).

The experimental phase contours have two distinct spacings in each element (narrower at higher applied fields and wider close to remanence). These different spacings are associated with the presence of ferromagnetic and antiferromagnetic coupling between the Ni and Co layers, as discussed below. Measurement of the phase-contour separations for both of these two coupled states implies that the thicknesses of each of the magnetically active layers was close to 3 nm, rather than the nominal 10 nm expected from calibration of the electron-beam evaporator used for film deposition. Processing the holograms to extract the mean inner potential contribution to the holographic phase confirmed that the thicknesses of the individual layers were approximately correct, so that over half of each magnetic layer was magnetically dead. Oxidation during lithographic processing is the most likely origin of this discrepancy.

The closest match with the experimental results was achieved for FM layer thicknesses of 3.5 nm, in close agreement with the thickness estimates based on the experimental phase contours. The corresponding simulations for each set of element shapes for 3.5-nm-thick magnetic films are shown in the remaining columns of Fig. 2. The columns labeled ''Co'' and ''Ni'' track the magnetization states of the individual FM layers within each element during the hysteresis cycle, while those labeled ''total'' show the computed holographic phase shifts, which can be compared directly with the experimental data. Changes in the total contour spacings are apparent between fields at which the Ni layer has reversed but the Co layer is still unchanged; similar behavior is

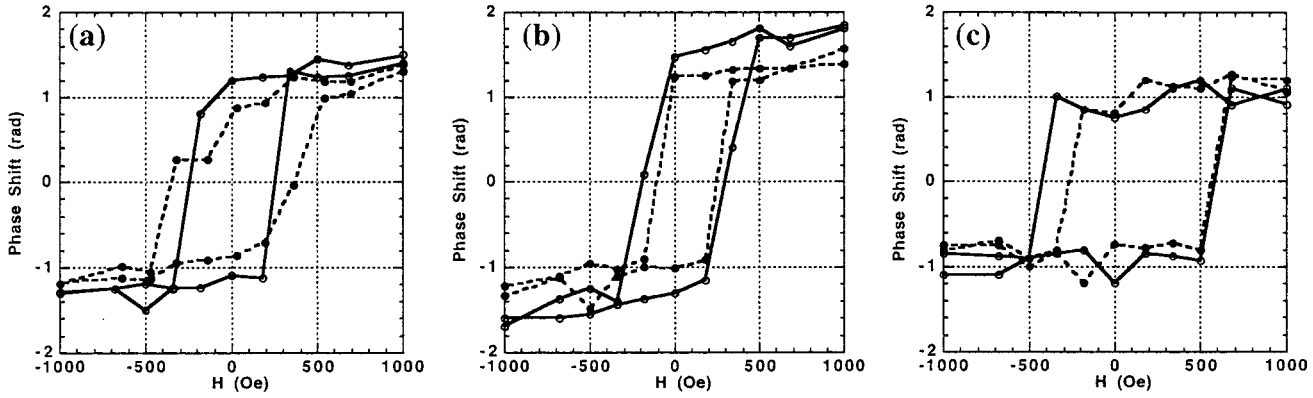

FIG. 3. Experimental phase differences measured across patterned Co/Au/Ni trilayer structures during complete hysteresis cycle:(a) diamonds, (b) ellipses, (c) rectangular bars. Solid/dashed lines correspond to larger/smaller elements, respectively.

also visible in each experimental hysteresis cycle (see discussion below).

Careful examination of the simulations for the individual FM elements as well as for the composite structures provides further insight into the magnetization reversal process. The most important result is that the Ni layer in each element reverses its magnetization well before the external field reaches 0 Oe, confirming that an antiferromagnetically coupled state is the normal remanent state that would be obtained after saturation of the element followed by removal of the external field. This antiferromagnetic (AFM) coupling must be due to the flux closure associated with the strong demagnetization field of the closely adjacent and magnetically more massive Co layer (higher $M_s t$ product, where t is the layer thickness). The darker yellow color of the Ni layer relative to that of the Co indicates that its magnetization is being pulled out-of-plane both by the externally applied field and by the strong Co demagnetization field.

The domain structures observed here in these extremely small, coupled magnetic structures clearly differ markedly from those seen in larger elements and single film structures. For example, the switching fields of the Ni and Co elements are sensitive to their thickness and shape, as well as the saturation magnetization of each layer. The occurrence of flux closure associated with an antiferromagnetic remanent state contributes to a lack of end domains. This contrasts with the behavior observed in thicker single layer films in which end domains help to eliminate the external stray fields that would lead to significantly higher free energies. We have previously reported that larger Co nanostructures of 30 nm thickness have solenoidal domain structures over a wide range of applied fields,[6] and similar magnetization vortices have been reported to cause anomalous switching behavior in 20-nm-thick NiFeCo submicron arrays.[14] Configurations resembling the remanent ''*S*'' and ''*C*'' states simulated in Ref. 2 for a single Co layer can be recognized for the bar-shaped element, for example, at -336 and $+168$ Oe, respectively, but these configurations are not the remanent states for this coupled system.

The switching behavior of several of the trilayer elements is compared in the form of hysteresis loops in Figs. 3 and 4. The experimental loops in Fig. 3 were obtained by plotting the magnetic contribution to the total phase difference across the mid-point of each element, as measured directly from the holographic phase contours. For both the diamond- and elliptical-shaped elements, there is a small but noticeable decrease in the phase soon after the external magnetic field is reduced in strength. This phase decrease is con-

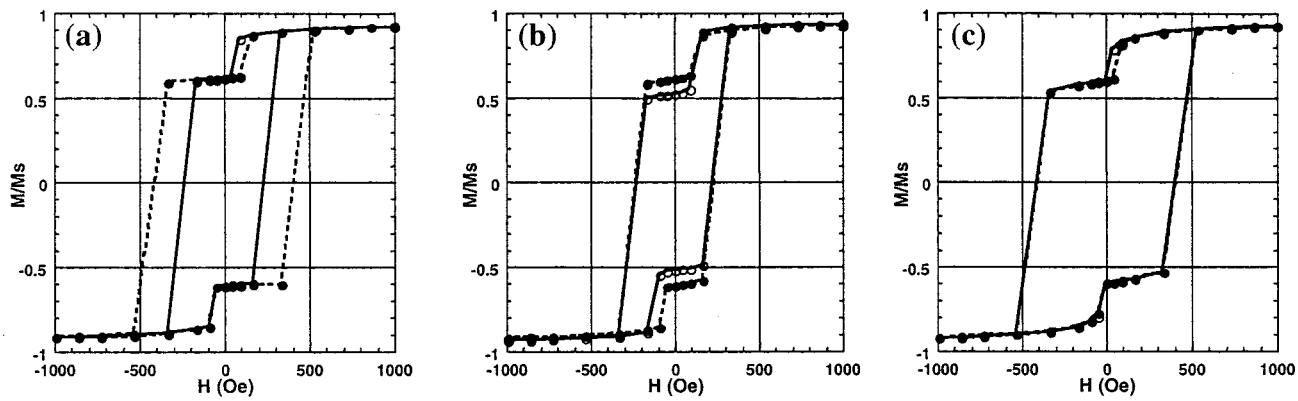

FIG. 4. Hysteresis loops derived from micromagnetic simulations for patterned elements: (a) diamonds, (b) ellipses, (c) rectangular bars. Solid/dashed lines correspond to larger/smaller elements, respectively.

sistent with the magnetization of the Ni layer being gradually pulled out of the plane before field reversal occurs. Note also that the major Co switching field for the bar-shaped elements is considerably larger than for the other element shapes, which is presumably due to the difficulty of nucleating reversal in a thin narrow element in the absence of end-domain structures.[11]

The simulated loops in Fig. 4 show the fractional magnetization M/M_S (where M_S is the saturation magnetization in the direction of the applied field), as computed for both smaller and larger elements of each shape. The drop in magnitude that occurs in these simulations before 0 Oe corresponds to the reversal of the Ni layers but the drop is later and more abrupt than observed experimentally, perhaps reflecting some variability in grain size and orientation in the experimental Ni film that helps to facilitate earlier reversal. The square shape for the Co switching in both the experimental and simulated loops provides further evidence for the absence of end domains which are reported to affect the behavior of large rectangular elements.[13] It is also interesting that the smaller of the two diamond-shaped elements has a substantially larger switching field, similar to that of the bar-shaped element. Similar increases in switching field with decreasing element width have been reported previously for thin Co nanoelements,[11] and have been attributed to the increased difficulty of nucleating magnetization reversal.

A significant outcome of this study is the agreement between the computed and measured phase contour maps, particularly in the ferromagnetically and antiferromagnetically coupled regimes. The Co element reverses its magnetization experimentally at the correct coercive field, although the Ni switches earlier and more gradually than expected from the simulations. A slight left-right asymmetry is also observed experimentally, possibly due to slight irregularities in the element shapes or thicknesses. The importance of acquiring high quality experimental data is highlighted by the sensitivity of the simulations to a large number of variables. The diamond- and elliptical-shaped elements examined were large enough to support vortices experimentally but we were unable to form them in the computations without artificial means (roughness, large magnetization fluctuations, etc.) during evolution from the saturated state. Experimental factors such as crystal grain size and orientation are likely to have an increasing influence on domain configurations in future generations of even smaller elements. The reproducibility of the domain structure in successive hysteresis cycles will also become an important consideration, and may possibly be overcome by careful attention to element shape and aspect ratio. The remanent AFM coupling of closely spaced FM layers will also be of particular relevance in practical device applications.

ACKNOWLEDGMENTS

This work was partly supported by an IBM subcontract on the DARPA Advanced MRAM Project under Contract No. MDA-972-96-C-0014. The authors thank James Speidell at IBM for providing Si_3N_4 membranes, and they acknowledge use of facilities in the Center for High Resolution Electron Microscopy at Arizona State University.

[1] J. N. Chapman, P. R. Aitchison, K. J. Kirk, S. McVitie, J. C. S. Kools, and M. F. Gillies, J. Appl. Phys. **83**, 5321 (1998).
[2] Y. Zheng and J.-G. Zhu, J. Appl. Phys. **81**, 5470 (1997).
[3] Y. Lu, R. A. Altman, A. Marley, S. A. Rishton, P. L. Trouilloud, G. Xiao, W. J. Gallagher, and S. S. P. Parkin, Appl. Phys. Lett. **70**, 2610 (1997).
[4] S. S. P. Parkin, Annu. Rev. Mater. Sci. **25**, 357 (1995).
[5] R. E. Dunin-Borkowski, M. R. McCartney, B. Kardynal, and D. J. Smith, J. Appl. Phys. **84**, 374 (1998).
[6] R. E. Dunin-Borkowski, M. R. McCartney, B. Kardynal, D. J. Smith, and M. R. Scheinfein, Appl. Phys. Lett. **75**, 2641 (1999).
[7] M. R. Scheinfein, J. Unguris, J. L. Blue, K. J. Coakley, D. T. Pierce, R. J. Celotta, and P. J. Ryan, Phys. Rev. B **43**, 3395 (1991).
[8] M. R. McCartney, D. J. Smith, R. F. C. Farrow, and R. F Marks, J. Appl. Phys. **82**, 2461 (1997).
[9] R. E. Dunin-Borkowski, M. R. McCartney, D. J. Smith, and S. S. P. Parkin, Ultramicroscopy **74**, 61 (1998).
[10] Y. Zheng and J.-G. Zhu, J. Appl. Phys. **85**, 4776 (1999).
[11] M. Ruhrig, B. Khamsepour, K. J. Kirk, J. N. Chapman, P. R. Aitchison, S. McVitie, and C. D. Wilkinson, IEEE Trans. Magn. **32**, 4452 (1996).
[12] K. J. Kirk, J. N. Chapman, and C. D. W. Wilkinson, Appl. Phys. Lett. **71**, 539 (1997).
[13] J. Shi, T. Zhu, M. Durlam, E. Chen, S. Tehrani, Y. F. Cheng, and J.-G. Zhu, IEEE Trans. Magn. **34**, 997 (1998).
[14] J. Shi, S. Tehrani, T. Zhu, Y. F. Zheng, and J.-G. Zhu, Appl. Phys. Lett. **74**, 2525 (1999).